Zhang *et al. Biochar* (2025) 7:82
https://doi.org/10.1007/s42773-025-00474-y

Biochar

ORIGINAL RESEARCH Open Access

Atmosphere regulation: unraveling effective strategies for creating high-performance iron ore/biochar composite nanomaterials in ball milling processes

Hui Zhang[1], Zi Cheng[1], Kai Hu[1], Boxiong Shen[1], Honghong Lyu[1*] and Jingchun Tang[2*]

Abstract

Ball milling technology has become an important method for material modification due to its high efficiency, environmental protection and economy. However, previous studies mainly focused on the adjustment of ball milling parameters and lacked an in-depth understanding of the effect of ball milling atmosphere on material properties. To this end, siderite/biochar composites (BM-SD/BCs) were prepared by ball milling technique and the effects of different ball milling atmospheres (air, nitrogen, vacuum) on the physicochemical properties of the composites and their catalytic performance were systematically investigated. The results showed that the N/BM-SD/BC prepared under nitrogen atmosphere exhibited excellent catalytic performance in phenol removal efficiency of 90.3%, which was significantly higher than that of the A/BM-SD/BC prepared under air atmosphere (73.8%) and the V/BM-SD/BC prepared under vacuum atmosphere (81.3%). Characterization analysis revealed that the ball milling treatment markedly altered the surface morphology and structural properties of the composites. Specifically, the composites ball-milled under nitrogen atmosphere exhibited smaller particle sizes, larger specific surface area (ascending from 27.0 to 187.6 $m^2 g^{-1}$), and richer distribution of surface functional groups and Fe(II) species. All these characteristics significantly enhanced their redox activities. This structural optimization not only increased the active sites of the composites, but also effectively enhanced their activation of persulfate (PS), which was capable of generating a variety of reactive radicals (such as $SO_4^{\cdot-}$, $^{\cdot}OH$, and $^{\cdot}O_2^-$) for the efficient degradation of phenol, in which $^{\cdot}OH$ and $^{\cdot}O_2^-$ contributed 50.7% and 25.3% of phenol removal, respectively. In addition, the N/BM-SD/BC/PS system demonstrated its capability to degrade phenol across a broad pH spectrum (especially in the pH range of actual wastewater), showing good adaptability and potential for practical application. This study reveals the key role of ball milling atmosphere in the modulation of material physicochemical properties and reactivity, which provides theoretical support for the future application of ball milling in the engineering of nanomaterials.

Highlights

- Milling atmosphere affected the morphology, functional groups and Fe(II) distribution of composites.
- Nitrogen atmosphere-prepared composite had the best specific surface area and Fe(II) distribution.
- Nitrogen atmosphere better than air/vacuum aided particles fracture and functional groups exposure.
- In N/BM-SD/BC/PS system, phenol oxidation was mainly by ·OH (50.7%) and $^{\cdot}O_2^-$ (25.3%).

*Correspondence:
Honghong Lyu
honghonglyu@hebut.edu.cn
Jingchun Tang
tangjch@nankai.edu.cn
Full list of author information is available at the end of the article

Keywords Siderite, Biochar, Ball mill, Atmosphere, Persulfate

Graphical Abstract

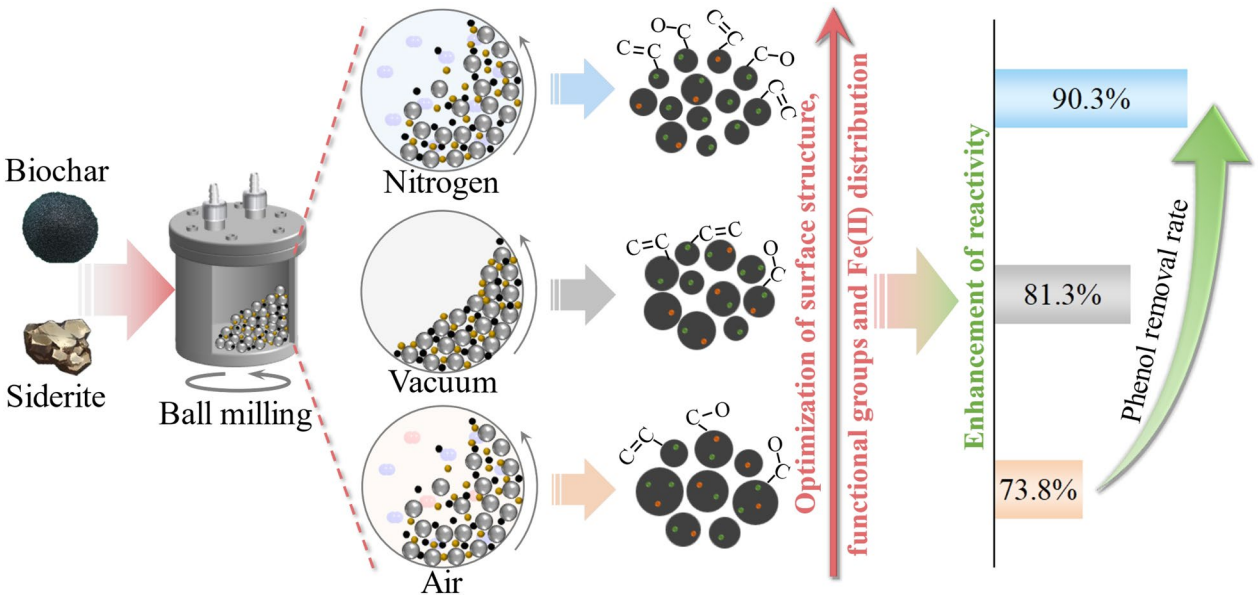

1 Introduction

High-energy ball milling, characterized by mild reaction conditions, high efficiency, low energy consumption, and technical and economic feasibility, has become a widely used technique for engineering modification of nano (composite) materials (Kumar et al. 2020; Lyu et al. 2017a; Naghdi et al. 2017; Gao et al. 2024). So far, a variety of materials based on ball milling have been successfully synthesized and applied in water purification, including activated carbon (Nasrullah et al. 2021), carbon nanotubes (Cheng et al. 2024), zero-valent iron (Sun et al. 2024) and their modified composites, especially biochar (BC) (Lyu et al. 2018a). The ball milling technology induces particle diffusion and dissolution during collisions and compaction, which promotes chemical reactions (Wang et al. 2023). These reactions can significantly alter the structure and properties of the materials, thereby enhancing the reactivity of the resulting composites (Yang et al. 2022). As in our previous study, iron disulfide (FeS_2) was successfully incorporated with BC via ball milling, and the BC inhibited the agglomeration of FeS_2, resulting in 3–25 times increase in the removal of Cr(VI) by the composites, in comparison to original and ball-milled BC and FeS_2 (Tang et al. 2021). This highlights the potential of ball milling in modulating material properties. However, traditional optimization of ball-milled materials has primarily focused on adjusting process parameters, such as increasing the milling speed or introducing chemical agents to modify material characteristics (Wang et al. 2023; Ma et al. 2024; Cheng et al. 2022). Innovative methods for systematically controlling and fine-tuning the properties of ball-milled nanocomposites are still lacking, especially outside of these traditional approaches.

Recent studies have emphasized the importance of atmospheric conditions during ball milling, which serve as a key factor influencing the physicochemical properties of the milled materials, yet remain underexplored (Liu et al. 2024). Different atmospheric conditions, including air, nitrogen, and vacuum, can significantly affect the structure and adsorption/catalytic properties of the resulting materials. For example, Xu et al. found that nitrogen and vacuum atmospheres are more conducive to reducing the particle size of ball-milled biochar compared to air (Xu et al. 2021). During air-atmosphere milling, the oxidation process of oxygen and the binding of heteroatoms to carbon structure increase the oxygen-containing functional groups of BCs. In contrast, ball milling in an oxygen-deficient atmosphere (such as nitrogen or vacuum) inhibits the formation of these functional

groups (Kumar et al. 2020). Moreover, surface functional groups play a significant role in determining the environmental performance of ball-milled materials (Lyu et al. 2018a; Xiao et al. 2020a). For instance, the introduction of oxygenated functional groups such as carboxyl groups (–COOH) and hydroxyl groups (–OH) may have adverse effects on pollutant removal due to their primarily negative charge at natural pH, which can lead to electrostatic repulsion between the material and anionic pollutants like hexavalent chromium or pentavalent arsenic, thereby inhibiting pollutant removal (Yang et al. 2019). Despite these observations, there is still insufficient understanding of how atmospheric conditions during high-energy ball milling can alter the properties and reactivity of nanocomposites, and the underlying mechanisms of this modulation remain unclear.

Especially when variable iron ore is involved, it can further complicate the system. Iron (Fe), a common component in many catalytic materials, exists in various oxidation states, with Fe(II) and Fe(III) being the most prevalent (Huang et al. 2021). The redox flexibility of Fe makes it a hot material for modifying biochar and applying it in advanced oxidation processes (AOPs), such as persulfate (PS) activation (Rong et al. 2019; Dong et al. 2017). PS is a widely used oxidant for environmental remediation and can be activated by Fe(II) in iron ore to generate highly reactive sulfate radicals ($SO_4^{-\cdot}$, Eqs. (1)-(3)), which effectively degrade a variety of organic pollutants, including phenol (Lee et al. 2020; Xiao et al. 2020b; Giannakis et al. 2021). Meanwhile, the large number of oxygen-containing functional groups, such as –OH and –COOH, possessed by biochar as a support material can be used as an electron donor to facilitate the electron transfer between the catalyst and PS in AOPs (Dai et al. 2019; Liu et al. 2020). Therefore, combining iron ore with biochar can improve the performance of its composites and increase the overall efficiency of AOPs. However, increasing or maintaining the Fe(II) content in the materials is critical because Fe(III) is less active in persulfate activation and Fe(II) is readily oxidized to Fe(III) under aerobic conditions (Zhang et al. 2019). This raises a key question: can an anoxic ball milling atmosphere retain Fe(II) in iron ore/biochar composites to enhance their catalytic activity? Based on this, it can be hypothesized that oxygen in the air atmosphere may promote the oxidation of Fe(II) to Fe(III), whereas nitrogen or vacuum atmospheres may retain a higher proportion of Fe(II), which in turn may improve the activation efficiency of PS.

$$\mathrm{Fe(II)} + \mathrm{S_2O_8^{2-}} \rightarrow \mathrm{Fe(III)} + \mathrm{SO_4^{-\cdot}} + \mathrm{SO_4^{2-}} \quad (1)$$

$$\mathrm{Fe(II)} + \mathrm{HSO_5^-} \rightarrow \mathrm{Fe(III)} + \mathrm{SO_4^{-\cdot}} + \mathrm{HO^-} \quad (2)$$

$$\mathrm{Fe(II)} + \mathrm{HSO_5^-} \rightarrow \mathrm{Fe(III)} + \mathrm{SO_4^{2-}} + {}^{\cdot}\mathrm{OH} \quad (3)$$

To verify this hypothesis, this study selected phenol, a persistent organic pollutant, as a model contaminant, and used siderite ($FeCO_3$), a naturally occurring mineral, along with environmentally friendly biochar as research subjects. Siderite/biochar composites were prepared via ball milling under air, nitrogen, or vacuum atmosphere, and the catalytic performance of these composites in persulfate activation and phenol removal was investigated to explore the effects of milling atmospheres. This study aimed to (1) determine the physicochemical properties of the ball-milled siderite/biochar composites prepared under different atmospheres; (2) evaluate the performance of the different composites in activating PS to degrade phenol; and (3) elucidate the potential mechanisms underlying the changes in the physicochemical properties and PS activation performance of the composites prepared under different milling atmospheres. The results of this study will provide a deeper understanding of how ball milling parameters, particularly atmospheric conditions, can be utilized to optimize the design and performance of nanocomposites in environmental applications.

2 Materials and methods

2.1 Materials

In this work, all chemicals used were of analytical grade and all sample solutions were prepared with deionized water. Phenol, methanol (METH), tert-butyl alcohol (TBA), chloroform (CF), L-histidine (L-His), methyl phenyl sulfoxide (PMSO), methyl phenyl sulfone ($PMSO_2$), dimethyl sulfoxide (DMSO), 2,2,6,6-tetramethyl-4-piperidinol (TEMP), and 5,5-dimethyl-1-pyrolin-N-oxide (DMPO) were acquired from Kmart Chemical Technology Co., Ltd. (Tianjin, China). Sodium persulfate (PS) was sourced from Jiangtian Chemical Technology Co., Ltd. (Tianjin, China). The natural siderite (SD) was obtained from Haoyu Stone Trade Firm (Guangzhou, China) in lump form, crushed and sieved through a 100-mesh sieve before use. Feedstock biomass for pristine biochar and composite production, pine sawdust, was first washed three times with deionized water to remove surface impurities, air-dried, and then sieved through the 1 mm sieve.

2.2 Preparation of BM-SD/BC composite

Biochar was produced according to the methodology of our previous study (Lyu et al. 2018b, 2017b). Briefly, sieved pine sawdust was firstly dried in an oven at 80 °C

for 12 h, and afterwards put into an atmosphere furnace (SQLF-1200, Shanghai Jujing Precision Instrument Manufacturing Co., Ltd, Shanghai, China) for 2 h of slow pyrolysis under nitrogen atmosphere at 700 °C to produce biochar. The biochar obtained was labeled as BC and used to prepare BM-SD/BCs.

To investigate the influences of different ball-milling atmospheres on composites, BM-SD/BC was prepared in air, nitrogen and vacuum atmosphere, respectively. The method for the ball-milling was similar to previous studies (Lyu et al. 2018a; Xu et al. 2021). 1.8 g mixture of siderite and biochar (siderite to biochar mass ratio = 1:1) and 180 g of steel balls (diameter = 5 mm) were placed in a stainless-steel jar (250 mL) to be positioned in the ball mill (F-P4000, Focucy Experimental Instrument Co., Ltd., Hunan, China). After the atmosphere in the stainless-steel jars was air, nitrogen (pumping nitrogen for 20 min) and vacuum (vacuuming with the vacuum pump), respectively, ball milling was operated (running at 300 rpm for 12 h, changing the direction of rotation every 3 h). The resulted ball-milled composites were named as A/BM-SD/BC, N/BM-SD/BC, V/BM-SD/BC, respectively. To investigate the impact of the mass ratio of siderite to biochar on the catalytic properties, the N/BM-SD/BC composites with predetermined ratios (the mass ratios of siderite to biochar = 1:5, 1:3, 1:1, 3:1, 5:1) were prepared under nitrogen atmosphere (other conditions were the same).

2.3 Characterizations

The morphology and elemental distribution (C, O, and Fe) of the samples were characterized using scanning electron microscope (SEM) and energy dispersive spectrometer (EDS). The particle size distribution of the materials was measured using the centrifugal sedimentation particle size analyzer (BT-1500, Bettersize, Liaoning, China). The crystalline composition of material was analyzed using X-ray diffraction (XRD) to verify whether the composites had the structural features of the original components. The elemental composition and chemical state of the materials were examined by X-ray photoelectron spectroscopy (XPS), and the surface functional groups existing in the materials were analyzed using fourier transform infrared spectroscopy (FTIR). The electrochemical properties of the materials were evaluated by electron-accepting capacity (EAC), electron-donating capacity (EDC) and linear scanning voltammetry (LSV). Moreover, the samples were measured for specific surface area and zeta potential. Electron paramagnetic resonance (EPR) experiments were applied with DMPO and TEMP as the spin-trapping agent to detect the reactive oxygen species (ROS) produced during persulfate activation. The concentrations of PMSO and $PMSO_2$ were detected by high performance liquid chromatography (HPLC, Waters 1525). The reaction intermediates were detected by liquid chromatography-mass spectrometry (LC–MS, Agilent 1290 Infinity II, 6470 LC/TQ).

2.4 Degradation experiments

The experiments were all performed at room temperature. 1.0 g L^{-1} of each material (BC, SD, BM-SD/BCs) and 1.0 g L^{-1} of PS were added to a centrifuge tube containing phenol solution (50 mg L^{-1}), the tube was then placed in the rotary mixer with rotation rate at 70 rpm for 2 h. After that, fraction of samples was sampled and filtrated through 0.22 μm polyethersulfone (PES) membranes. According to 4-aminoantipyrine spectrophotometric method (HJ 503–2009), the concentrations of phenol were measured by ultraviolet–visible spectrophotometer (UV-1801, Beijing Beifen Ruili Analytical Instrument Co. Ltd, Beijing, China) at 510 nm. To determine the effect of he adsorption property of each material on phenol removal, the phenol adsorption experiment with only material (without PS) was conducted under the same reaction conditions. And the control experiment with PS alone was carried out for comparison. Furthermore, the optimal conditions of siderite-to-biochar mass ratio, PS dosage, material dosage and initial pH value were investigated. In addition, quenching experiments were performed to identify the role of active species in the system by adding TBA, METH, CF, L-His, PMSO, and DMSO as quenching agents, respectively.

3 Results and discussion

3.1 Effects of ball-milling atmosphere on the properties of BM-SD/BCs

In an attempt to systematically evaluate the impact of various ball milling atmospheres on the surface structure of biochar and its composites, the surface morphology of samples was characterized and analyzed by SEM. Based on the SEM images in Fig. 1a, it could be observed that the untreated biochar (BC) had complete and smooth surface structure with almost no tunneling and significant pores. However, the surface of ball-milled siderite-biochar composites (BM-SD/BCs) under different atmospheres underwent significant changes: all composites showed rough surfaces and micro- and nano-sized particle distributions (Fig. 1b–d). Further analysis by particle size statistics (Additional file 1: Fig. S1) showed that the N/BM-SD/BC composites had the smallest average particle size (3.02 μm), followed by V/BM-SD/BC (3.34 μm), while A/BM-SD/BC had the largest average particle size (3.66 μm). This observation suggested that the ball milling process significantly promoted particle fracture in both nitrogen and vacuum environments, but the vacuum environment might have generated negative

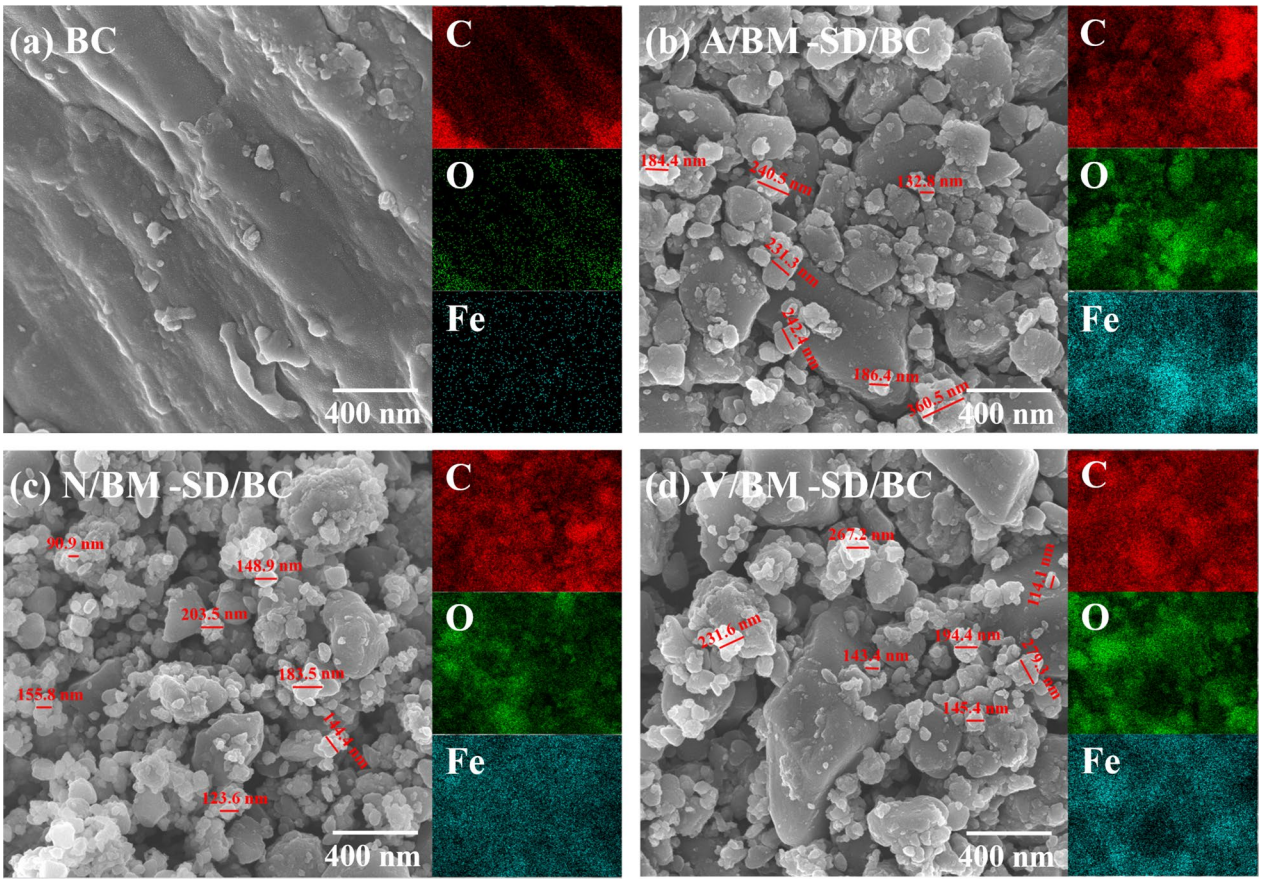

Fig. 1 SEM and EDS mapping of C, O and Fe elements of biochar and composites

pressure inside the sample vials, inhibiting further particle fracture, which is in agreement with prior research (Xu et al. 2021). Further, the elemental distributions of the material were affected as the surface morphology was significantly altered. To explore this, we used EDS mapping to analyze the distribution of iron in biochar and its composites. The findings revealed a marked enhancement in the iron content within the BM-SD/BCs in contrast to the BCs, with N/BM-SD/BC exhibiting the most uniform distribution of iron. This indicated that siderite was not only successfully loaded onto the surface of biochar, but also well dispersed in the composites prepared by ball milling under nitrogen atmosphere. This uniform distribution was important for improving the catalytic performance of the composites as it could maximize the interaction surface between the materials and the contaminants and oxidants and delivered more active sites for enhanced phenol removal.

Moreover, the pore structure characteristics of the BC and BM-SD/BCs were further revealed by nitrogen adsorption–desorption isotherm analysis (Additional file 1: Fig. S2a). Each sample exhibited typical IV isotherms accompanied by H3 hysteresis loops, suggesting that they mainly have mesoporous structures (Chen et al. 2024a). Combined with the porous structure parameters in Additional file 1: Fig. S2b and Table S1, the pore diameters of these samples were mainly concentrated between 3.82 and 6.75 nm, confirming their mesoporous properties. It was significant to mention that the composites (BM-SD/BCs) exhibited a markedly increased specific surface area and pore volume compared to the untreated BCs, aligning with the observations made through SEM analysis. However, the specific surface area of the three composites showed an inverse relationship with the particle size. The N/BM-SD/BC had a specific surface area of 187.6 m^2 g^{-1}, slightly, but not significantly, increased compared to A/BM-SD/BC (173.4 m^2 g^{-1}) and V/BM-SD/BC (175.5 m^2 g^{-1}). This might be attributed to the fact that a certain degree of agglomeration occurred between the nanoparticles during ball milling under nitrogen environment (as shown in Fig. 1c), which partially suppressed the effect of specific surface area increase. Therefore, the effect of particle fracture on specific surface area during ball milling was

twofold: (1) as particle size diminished, the specific surface area increased correspondingly; and (2) the clustering of particles resulted in a decline of the specific surface area. Nonetheless, the composites prepared by ball milling were able to provide greater number of active sites to promote the PS activation, thus accelerating the phenol degradation process.

To further explore the crystal structure variations of the composites, the crystal structures of biochar, siderite and their composites were analyzed by XRD (Fig. 2a). In the BC samples, the wide peaks near 23.0° and 43.0° were attributed to the diffraction peaks of the carbon structure, while the distinct diffraction peak appearing at 26.6° corresponded to silica (SiO_2) (Tang et al. 2021). For siderite, the diffraction peaks at 24.8°, 32.0°, 42.3°, and 52.8° characteristically indicated that its main constituent was iron carbonate ($FeCO_3$), in accordance with JCPDS No. 29–0696 (Zhong et al. 2023). Additionally, siderite contained small amount of pyrite (FeS_2) as a consequence of the fact that siderite is usually co-occurring with pyrite, whose diffraction peaks appeared at positions such as 33.1° and 56.3° (JCPDS No. 42–1340) (Chen et al. 2024b). In the siderite-biochar composites ball-milled under different atmospheres, the characteristic diffraction peaks of BC almost completely disappeared or were significantly weakened, probably due to the strong diffraction effect of Fe covering the diffraction peaks of carbon (Sun et al. 2024; Meng et al. 2022). However, the characteristic peaks of siderite remained distinctly discernible in the composites with significantly enhanced intensity. This change might be attributed to the fact that the ball milling process did not break the structural stability of siderite, but instead increased the exposed surface area of siderite, which, together with the supporting effect of biochar, led to its homogeneous distribution in the composites, thus contributing to the enhancement of the intensity of the characteristic peaks of siderite (Acisli et al. 2017). Meanwhile, it was confirmed that siderite could be successfully loaded and tightly bound to the biochar matrix through the ball milling process.

FTIR spectroscopy was utilized for the detection of major functional group characteristics in different materials. As in Fig. 2b, for pristine BC, the functional groups were decomposed or reorganized due to the high-temperature pyrolysis (700 °C) experienced during the preparation process, resulting in a relatively small number of functional group types, which were mainly characterized by –OH (3422 cm^{-1}) and C–O–C (1090 cm^{-1}) functional groups (He et al. 2019). The flat peak at about 3420 cm^{-1} of siderite was predominantly associated with the stretching vibration of the –OH bond, while the one at 1430 cm^{-1} was indicative of the C–O stretching vibration. Furthermore, the peaks observed at 864 cm^{-1} and 740 cm^{-1} indicated the stretching and bending vibrations of CO_3 (Zhong et al. 2023). Upon the combination of biochar and siderite through ball milling, the FTIR spectra of the composites not only retained the original functional groups of the two, but also showed new absorption

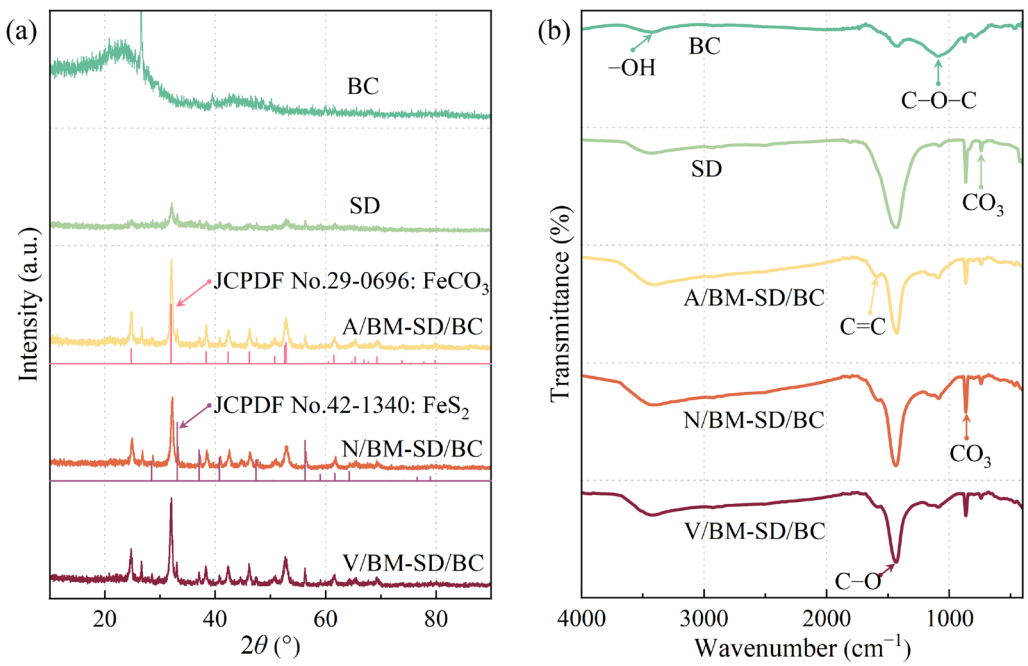

Fig. 2 XRD (**a**) and FTIR (**b**) of biochar, siderites and composites

peaks at 1588 cm^{-1}, which represented the C=C bond stretching vibration. This indicated that the functional groups on the surfaces of both were retained during the ball milling process, especially in the nitrogen atmosphere. Also, the ball milling treatment could incorporate new functional groups onto the surface of the material or expose the functional groups that were originally masked (Lyu et al. 2018b). Further analysis showed that the detection of C=C and C–O functional groups on the surface of composites suggested the incorporation of sp^2 hybrid structures (π-electrons) and oxygen-containing functional groups (e.g., C–OH) within the materials, thereby aiding in enhancing the activation process of PS (Duan et al. 2015). In addition, the composites prepared by ball milling under different atmospheres also exhibited changes in functional groups. As could be seen from Fig. 2b, the intensity of the characteristic peaks of N/BM-SD/BC was higher than that of A/BM-SD/BC and V/BM-SD/BC, and this discrepancy might be due to the nitrogen atmosphere being more conducive to the fracture and bonding of the particles, thereby exposing more functional groups. It might also be attributed to the protective effect of nitrogen on the structure of the material, avoiding excessive oxidation during ball milling and thus retaining more functional groups.

XPS analysis was employed to explore the elemental composition and its chemical state of the surface of the material. As depicted in Fig. 3a and detailed in Additional file 1: Table S2, the XPS spectrum of BC revealed that its surface was primarily composed of carbon (C) and oxygen (O) elements. The peaks labeled as C1*s* and O1*s* occupied 87.64% and 10.35% at 284.82 eV and 532.11 eV, respectively. In contrast, BM-SD/BCs loaded with siderite by ball milling were mainly composed of three elements, namely C, O and Fe. Among them, the relative contents of oxygen and iron increased significantly to 20.17–22.66% and 4.44–4.87%, respectively, indicating that siderite was effectively incorporated onto the surface of biochar. In particular, the surface oxygen content further increased to 32.65% after N/BM-SD/BC was involved in PS activation for phenol degradation, which is consistent with the trend observed in other studies on carbon nanomaterials, suggesting that the surface oxidation process was experienced during the N/BM-SD/BC reaction (Zhang et al. 2020). This oxidation might be related to the fact that the surface of N/BM-SD/BC was enriched with functional groups with electron transfer functions, which could participate in electron transfer during PS activation, leading to the oxidation of the material. In addition, N/BM-SD/BC was situated in an environment of intense oxidation, rich in free radicals and reactive intermediates, which might have further boosted the rate of oxidation occurring on the surface of the material, culminating in a significant increase in the oxygen content (Tang et al. 2018).

In order to further understand the effect of ball milling atmosphere on functional groups of BM-SD/BCs and their elemental changes and surface chemistry during the catalytic process, detailed analysis was conducted on high-resolution spectra of C1*s* and Fe2*p*. Figure 3b shows the distribution of functional groups on the surfaces of BM-SD/BCs, in which the summed C–O (285.53 eV) and O–C=O/C=O (288.32 eV) ratios of A/BM-SD/BC were higher, which might be related to the direct involvement of oxygen in the atmosphere; the presence of oxygen not only enhanced the oxygen-containing functional groups

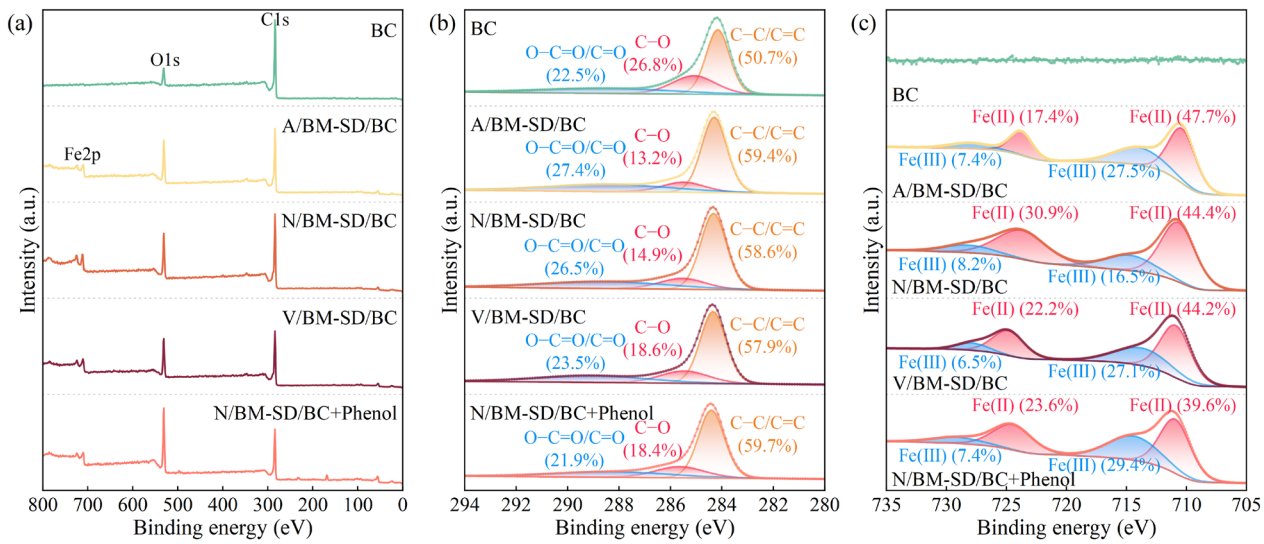

Fig. 3 XPS spectra of the BC and BM-SD/BCs before and N/BM-SD/BC after reaction with phenol: **a** survey, **b** C1*s*, **c** Fe 2*p* spectra

on the surfaces, but also might have affected the stability and activity of these functional groups in the stability and activity in the catalytic reaction. In contrast, in N/BM-SD/BC and V/BM-SD/BC, the ratio of C–C/C=C was higher, and the total contents of C–O and O–C=O/C=O were relatively reduced. These changes indicated that the anoxic atmospheres (nitrogen and vacuum atmospheres) could effectively inhibit the generation of some oxygen-containing functional groups and also made the surface more conducive to the activation reaction of PS by stabilizing the π-electron system (C=C) (Zhang et al. 2020). After the activation of N/BM-SD/BC for the degradation of phenol by PS, the relative proportion of C–C/C=C increased, but the proportion of C–O and O–C=O/C=O functional groups observed a decline. This change indicated that the functional groups were involved in electron transfer or bond rearrangement during the catalytic reaction and were transformed during the reaction.

In addition, Fe2*p* spectral analysis (Fig. 3c) revealed the effect of the ball milling atmosphere on the chemical state of Fe. It was found that the highest Fe(II) content was found in N/BM-SD/BC (73.4%), followed by V/BM-SD/BC (67.0%) and A/BM-SD/BC (62.8%). This trend suggested that ball milling treatment with nitrogen and vacuum atmospheres helped to reduce the oxidation of Fe(II) to Fe(III), thus maintaining higher levels of reduced Fe species. This finding was particularly important for the activation of PS, since Fe(II) is an efficient electron donor, which significantly improves the electron transfer efficiency and facilitates the activation of PS in phenol degradation (Xiao et al. 2020b). After participating in the activation of PS for phenol degradation, the proportion of Fe(II) in N/BM-SD/BC decreased from 73.4% to 62.1%, while the proportion of Fe(III) increased from 26.6% to 37.9%. This transformation of Fe(II)/Fe(III) ratio further proved that Fe(II) plays a key role in PS activation and phenol oxidation.

3.2 Removal of phenol by BM-SD/BCs activated PS

To investigate how the effect of ball milling atmosphere on the physicochemical properties of BM-SD/BCs modulates their reactivity, the activated PS degraded phenol was used as an example to reveal the role of ball milling atmosphere in modulating the properties of BM-SD/BCs by comparing the performance of different BM-SD/BCs.

3.2.1 Selection of reaction system

The systems both without and with PS were constructed to investigate the effect of ball milling atmosphere on the performance of the materials in the activated PS degradation reaction of phenol (Fig. 4a). In the systems without PS, all types of catalysts (BC, SD, A/BM-SD/BC, N/BM-SD/BC, and V/BM-SD/BC) showed no significant phenol removal effects, among which N/BM-SD/BC prepared under nitrogen atmosphere exhibited the highest phenol removal rate of 22.9%. This result could be ascribed to the characteristics of N/BM-SD/BC, which included greater specific surface area, higher pore volume, and rich surface functional groups. These were the result of the modulation of the ball milling atmosphere, which contributed to the enhancement of its ability to adsorb and react with pollutants. In the with PS reaction systems, the phenol removal efficiency achieved by single PS was not satisfactory, indicating that reliance on PS alone did not spontaneously decompose the generated sulfate radicals ($SO_4^{-\cdot}$), and thus did not effectively degrade phenol. In comparison, the BC/PS system exhibited a slight enhancement in phenol removal, with an increase of merely 3.1%. This result might be due to the presence of oxygen-containing functional groups on the the surface of biochar, which were able to activate PS to some extent, forming catalytic sites or facilitating electron transfer to generate sulfate radicals, which in turn oxidatively degraded phenol (Thi-Hai Anh and Oh 2019). However, the original scarcity of biochar in the diversity of functional groups, along with its susceptibility to interference within complex environmental conditions, contributed to its underwhelming catalytic performance. In contrast, the phenol removal was enhanced to 20.0% in the SD/PS system. This was credited to the fact that Fe^{2+} in siderite could effectively activate persulfate and promote the degradation reaction of phenol. For the three composites (A/BM-SD/BC, N/BM-SD/BC, and V/BM-SD/BC), the introduction of PS significantly improved the phenol removal efficiency, which indicated the significant synergistic effect between BM-SD/BCs and PS in the catalytic degradation of phenol. BM-SD/BCs could efficiently activate PS to generate active species with higher oxidation potentials, including $SO_4^{-\cdot}$ and $^{\cdot}OH$, which enhanced the degradation rate of phenol. Especially noteworthy was that the N/BM-SD/BC/PS system exhibited the best phenol removal, indicating that the composites prepared by ball milling in nitrogen atmosphere possessed superior physicochemical properties and were more conducive to the activation of PS.

3.2.2 Effects of critical operational factors

For the siderite and biochar composites employed in activating PS to degrade phenol, tuning the critical operational factors was essential to enhance material efficacy. The main influencing factors included the mass ratio of siderite to biochar, the amount of composites, the dosage of PS, and the initial pH value. To deeply examine the influence of these factors on the composite activity, the

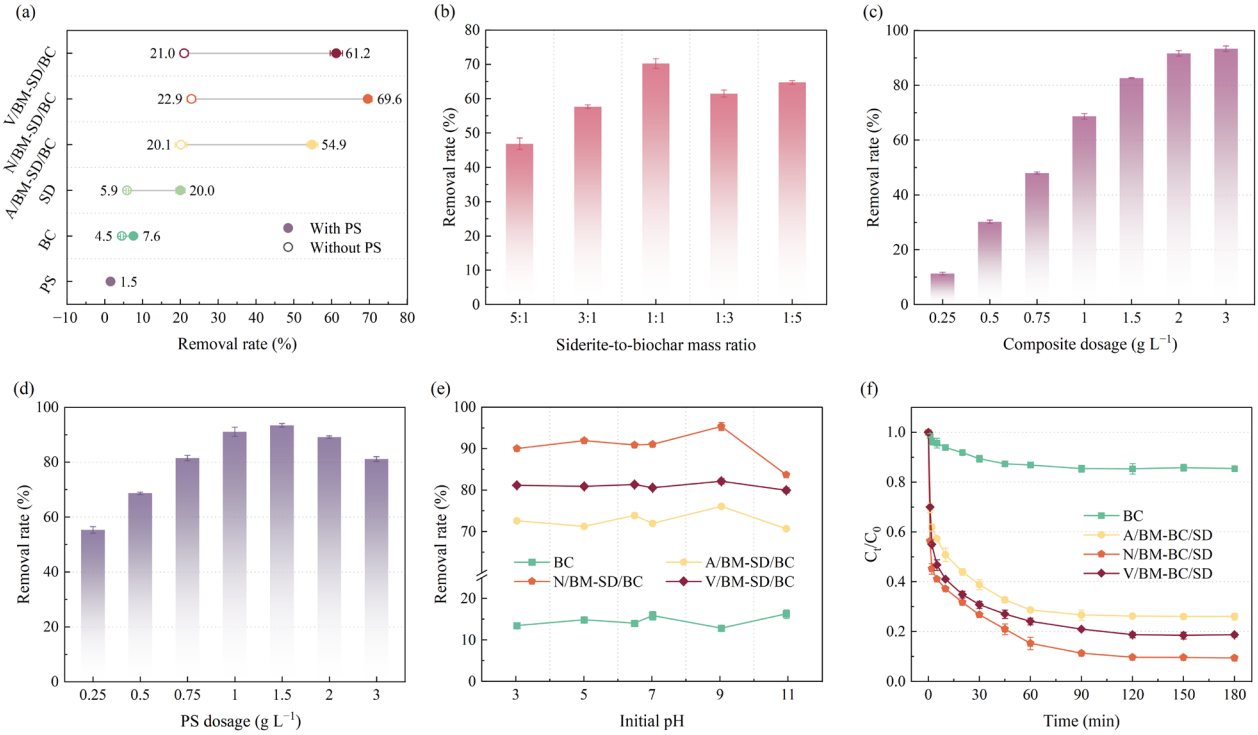

Fig. 4 Removal rates of phenol in different reaction systems **a** (Reaction conditions: $[BC]_0 = [SD]_0 = [BM\text{-}BC/SDs]_0 = 1.0$ g L^{-1}, $[PS]_0 = 1.0$ g L^{-1}, $[phenol]_0 = 50$ mg L^{-1}, initial pH = 6.5, reaction time = 120 min); Effect of siderite-to-biochar mass ratio in N/BM-BC/SD **b** (Reaction conditions: $[N/BM\text{-}BC/SDs]_0 = 1.0$ g L^{-1}, $[PS]_0 = 1.0$ g L^{-1}, $[phenol]_0 = 50$ mg L^{-1}, initial pH = 6.5, reaction time = 120 min,); Effect of N/BM-BC/SD dosage **c** (Reaction conditions: $[N/BM\text{-}BC/SD]_0 = 0.25$–$3.0$ g L^{-1}, $[PS]_0 = 1.0$ g L^{-1}, $[phenol]_0 = 50$ mg L^{-1}, initial pH = 6.5, reaction time = 120 min); Effect of PS dosage **d** (Reaction conditions: $[N/BM\text{-}BC/SD]_0 = 2.0$ g L^{-1}, $[PS]_0 = 0.25$–3.0 g L^{-1}, $[phenol]_0 = 50$ mg L^{-1}, initial pH = 6.5, reaction time = 120 min); Effect of initial pH **e** (Reaction conditions: $[BC]_0 = [BM\text{-}BC/SDs]_0 = 2.0$ g L^{-1}, $[PS]_0 = 1.0$ g L^{-1}, $[phenol]_0 = 50$ mg L^{-1}, initial pH = 3–11, reaction time = 120 min); Effect of reaction time **f** (Reaction conditions: $[BC]_0 = [BM\text{-}BC/SDs]_0 = 2.0$ g L^{-1}, $[PS]_0 = 1.0$ g L^{-1}, $[phenol]_0 = 50$ mg L^{-1}, initial pH = 6.5, reaction time = 0–180 min)

composite N/BM-SD/BC, which was the most effective in degrading phenol, was selected for this study.

Firstly, the mass ratio between siderite and biochar significantly affected the formation of the composites and their distribution of active sites. Figure 4b illustrates that the phenol removal efficiency varied significantly with different mass ratios of siderite to biochar in the composites. The composites achieved peak phenol removal efficiency at the mass ratio of siderite to biochar of 1:1. However, when the proportion of siderite was higher (i.e., at mass ratios of 3:1 and 5:1), the phenol removal efficiencies of the composites decreased significantly. This phenomenon could be explained by the fact that higher siderite ratios weakened the supporting role of biochar, thereby causing a decline in the specific surface area and porosity of composites, as well as reducing the availability of surface functional groups and reactive sites, which in turn reduced their ability in catalyzing the degradation of phenol through the activation of PS. On the contrary, when the proportion of biochar exceeded that of siderite (i.e., at mass ratios of 1:3 and 1:5), the phenol removal efficiency improved and continued to rise as the proportion of biochar increased. This suggested that the boost in phenol degradation efficiency was primarily influenced by the ability of biochar to adsorb phenol. Hence, the mass ratio of siderite to biochar at 1:1 was found to be the most effective combination for achieving the best phenol elimination.

Secondly, the dosage of composites was another key factor affecting the degradation efficiency. Figure 4c demonstrates that the phenol removal efficiency progressively improved as the dosage of N/BM-SD/BC was augmented. Specifically, as the dosage of N/BM-SD/BC rose from 0.25 to 2.0 g L^{-1}, there was a marked surge in the phenol removal efficiency, escalating from 11.2% to 91.6%. This observation was understandable given the fact that increasing the dosage of N/BM-SD/BC ensured more active sites to effectively contact with phenol and PS, thus improving the removal efficiency. However, upon raising the N/BM-SD/BC dosage to 3.0 g L^{-1}, the phenol removal rate saw only a marginal rise to 93.3%. This indicated that too much N/BM-SD/BC might lead to competition

among active sites, which not only decreased the reaction performance per unit mass, but also increased the treatment cost. Therefore, the optimal dosage was 2.0 g L^{-1}.

Furthermore, the incorporation of PS served as a critical determinant in modulating the performance of the degradation process. The concentration of PS directly affected the production of ROS throughout the activation phase, subsequently governing the efficiency of phenol degradation. Figure 4d illustrates that with the rise in PS concentration from 0.25 to 1.0 g L^{-1}, there was a corresponding increase in phenol removal from 55.2% to 91.0%. However, when the PS concentration reached 1.5 g L^{-1}, 2.0 g L^{-1}, and 3.0 g L^{-1}, the phenol removal did not increase significantly and even decreased. The reason for this could be that while higher concentrations of PS enhanced the utilization of active sites and produced an increased amount of ROS, excessive PS might undergo self-quenching and convert $^{\cdot}OH$ and $SO_4^{-\cdot}$ to $S_2O_8^{-\cdot}$ and oxygen with lower oxidative capacity (Eqs. (4)–(6)) (Wang et al. 2019). Therefore, it was reasonable to select a PS concentration of 1.0 g L^{-1} for subsequent studies in order to ensure high phenol removal while reducing the operating cost.

$$SO_4^{-\cdot} + S_2O_8^{2-} \rightarrow S_2O_8^{-\cdot} + SO_4^{2-} \quad (4)$$

$$^{\cdot}OH + S_2O_8^{2-} \rightarrow S_2O_8^{-\cdot} + OH^- \quad (5)$$

$$6H_2O + 4S_2O_8^{-\cdot} \rightarrow 8SO_4^{2-} + 3O_2 + 12H^+ \quad (6)$$

3.2.3 Effects of initial pH

It is well known that the solution pH value usually significantly impacts the behavior of redox systems, because it not only determines the charge characteristics of the material surface, but also affects the efficiency of PS decomposition and the formation of ROS. Therefore, the influence of initial pH on the catalyst/PS phenol removal system was examined without the use of a buffer, with the findings presented in Fig. 4e. The small differences in phenol degradation rates among the BM-BC/SD/PS systems across distinct initial pH values indicated that the system efficacy was relatively stable over wide pH range. This phenomenon might be attributed to the strong acidity of PS. Upon introducing PS and BM-BC/SDs into the solutions, the solutions pH rapidly decreased from 3–9 to 2.78–3.08. Similarly, the pH of solutions initially at the pH of 11 saw swift decline to 3.69–3.85, as depicted in Additional file 1: Fig. S3a. At this time, the pH of the solution was below the point of zero charge (PZC) for the BM-BC/SDs (Additional file 1: Fig. S3b), and the surface of the BM-BC/SDs carried positive charge, which contributed to the adsorption of negative ions of PS ($S_2O_8^{2-}$) via electrostatic interaction, thus enhancing the activation of the PS and realizing more rapid and efficient synergistic effect (Damiri et al. 2020). These results indicated that the oxidation process of PS could be carried out efficiently across broad spectrum of initial pH values (Yin et al. 2019). Therefore, the N/BM-S/BC/PS process is capable of degrading phenol effectively in practical applications, since the initial pH of real wastewater usually ranges from 5 to 9.

3.2.4 Effects of ball milling atmosphere on the catalytic performance of BM-SD/BCs

The experimental results showed that different ball milling atmospheres had a pronounced influence on the catalytic capabilities of BM-SD/BC composites in the phenol degradation reaction. Therefore, the influences of ball milling atmosphere on the catalytic performance of BM-SD/BC were deeply explored by comparing the performance of the composites prepared with three ball milling atmospheres in phenol removal under optimized reaction conditions. Figure 4f reveals that the pristine biochar (BC) exhibited low removal efficacy for phenol, achieving only 14.6%. However, all three composites prepared by ball milling significantly improved the phenol removal efficiency and reached equilibrium within 120 min. Particularly noteworthy was that the N/BM-SD/BC composites obtained by ball milling under nitrogen atmosphere exhibited excellent adsorption and catalytic activation properties, with phenol removal efficiencies as high as 90.3%, which were significantly better than those of A/BM-SD/BC prepared under air atmosphere (73.8%) and V/BM-SD/BC prepared under vacuum atmosphere (81.3%). Simultaneously, the detailed examination of phenol degradation levels across different catalytic systems was conducted via total organic carbon (TOC) analysis. According to the data in Additional file 1: Fig. S4, the TOC removal in the N/BM-SD/BC/PS system reached 69.6%, which was higher than that of the A/BM-SD/BC/PS system (53.6%) and the V/BM-SD/BC/PS system (58.5%). This result further confirmed that the catalytic performance of the N/BM-SD/BC composite was significantly better than the other two composites under nitrogen atmosphere. The reason for this was that the nitrogen atmosphere might have better preserved the key active sites in the materials throughout the ball milling and promoted the homogeneous dispersion of the metal components, which significantly improved the efficacy of PS activation and the subsequent breakdown of phenol. For example, the minimum particle size and maximum specific surface area of N/BM-SD/BC favored increased exposure of active sites (e.g., Fe(II) and oxygen-containing functional groups), which directly improved

its contact efficiency with PS. In contrast, composites ball-milled under air and vacuum atmospheres might not be as good as materials under nitrogen atmospheres in terms of distribution of active components and formation of active sites, which results in their lower catalytic performance. This difference in atmosphere ultimately determined the performance of the composites during persulfate activation by affecting their structural and chemical properties.

In addition, Additional file 1: Table S3 lists the experimental results of this study as well as previously published experiments on the degradation efficiency of different materials on organic pollutants. Upon comparative analysis, it could be seen that N/BM-SD/BC performed well in degrading phenol and showed significant advantages compared to previous studies. It was worth emphasizing thatin the present study, the effect of ball milling atmosphere on the physicochemical properties and catalytic performance of siderite/biochar composites was systematically investigated, and it was found that the composites prepared under nitrogen atmosphere performed excellently in the degradation of phenol by activated PS, revealing that the ball milling atmosphere can be used as an important variable to optimize the design of highly efficient environmental catalysts, thus providing new ideas for their design and optimization.

3.3 Mechanisms of activation of PS by BM-SD/BC prepared under different ball milling atmospheres

The ball milling atmosphere affected the reactivity of BM-SD/BCs in activating PS for phenol removal by influencing the physicochemical properties of BM-SD/BCs, which might also in turn affect the mechanism of their activation of PS. Therefore, the mechanism of PS activation by BM-SD/BCs under different ball milling atmospheres was explored.

3.3.1 Synergistic mechanisms of PS

Electrochemical characterization was used to verify the synergistic effect of PS. The oxidation and reduction current response curves of the different systems were compared (Additional file 1: Fig. S5a-c). In the presence of A/BM-SD/BC, V/BM-SD/BC, N/BM-SD/BC composites alone, it was found that N/BM-SD/BC had higher EDC and EAC. This result suggested that N/BM-SD/BC had stronger redox capacity and was more likely to donate electrons during the reaction process, which in turn efficiently activated the PS to produce free radicals, leading to a more effective degradation of phenol (Zhen et al. 2021). Meanwhile, the EAC and EDC of the BM-SD/BCs/PS systems were significantly higher than those of the PS or BM-SD/BCs systems alone, suggesting that there was synergistic effect between PS and BM-SD/BCs to promote electron transfer. Further, the EDC in BM-SD/BCs/PS/phenol increased significantly when phenol was introduced into the systems, indicating that phenol donated electrons and was oxidized during the reaction. In addition, it was also evident from the LSV curves (Additional file 1: Fig. S5d) that among the systems of the three composites with PS and phenol, the current was higher in the system of N/BM-SD/BC, which further confirms that N/BM-SD/BC had stronger electron transfer ability.

3.3.2 Identification of active species

Firstly, the generation of ROS in the reaction system was detected by EPR technique with DMPO and TEMP as the trapping agents, and the characteristic peaks of adducts of DMPO-OH (1:2:2:1), DMPO-$SO_4^{\cdot-}$ (1:1:1:1:1), DMPO-$O_2^{\cdot-}$ (six-lined peaks), and TEMP-$^1O_2$ (1:1:1) were examined. As depicted in Fig. 5a, the distinctive signals for $^{\cdot}OH$ and $SO_4^{\cdot-}$ radicals were successfully observed in the BC/PS system, which suggested that the pristine BC could activate the PS to generate radicals. This activation process might

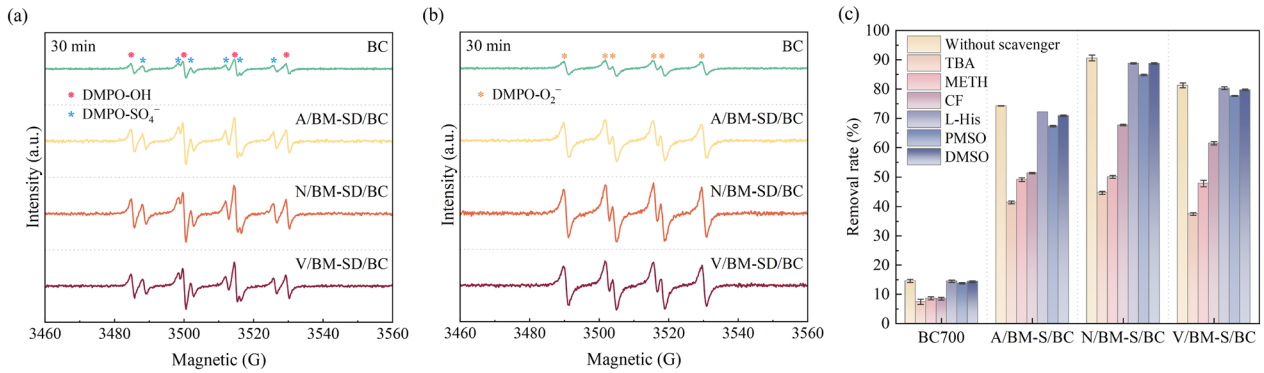

Fig. 5 EPR spectra of BC and BM-SD/BCs and PS systems in the presence of DMPO (**a**, **b**); the removal of phenol in the presence of different scavengers (**c**) (Reaction conditions: $[BC]_0 = [BM\text{-}BC/SDs]_0 = 2.0$ g L^{-1}, $[PS]_0 = 1.0$ g L^{-1}, $[phenol]_0 = 50$ mg L^{-1}, initial pH = 6.5, reaction time = 120 min)

be associated with the functional groups with oxygen (such as –OH, –COOH, etc.) present on the BC surface, which could serve as electron shuttles, facilitating the electron transfer process that enhances the breakdown of PS and the formation of radicals (Eqs. (7)-(8)) (Thi-Hai Anh and Oh 2019). The intensities of the characteristic peaks of DMPO-OH and DMPO-SO_4^- adducts were significantly enhanced in the BM-SD/BCs/PS systems, suggesting that the loading of siderite markedly improved the capacity of composites to activate PS to generate free radicals. Especially, the highest intensity of the characteristic peaks of free radicals was detected in the N/BM-SD/BC/PS system. This was attributed to its richer content of functional groups with oxygen and Fe(II) species. It was noteworthy that the intensities of DMPO-OH signals surpassed those of DMPO-SO_4^- in all four materials/PS systems, indicating higher $^{\cdot}OH$ content in the system, which might be associated with the transformation of $SO_4^{\cdot-}$ into $^{\cdot}OH$ (Eqs. (9)). In addition, six characteristic peaks belonging to superoxide radicals ($^{\cdot}O_2^-$) are clearly observed in Fig. 5b, which prove the existence of $^{\cdot}O_2^-$ within the system. Similarly, the intensity of characteristic peaks of DMPO-O_2^- adducts in the BM-SD/BCs/PS systems was significantly superior to that observed in the BC/PS system, especially in the N/BM-SD/BC/PS system. This further indicated that N/BM-SD/BC could activate PS efficiently and produced more free radicals. However, the TEMP-$^1O_2$ characteristic signal peak was not observed in any of the four materials/PS systems (Additional file 1: Fig. S6), which indicated that the ROS in the systems were mainly $^{\cdot}OH$, $SO_4^{\cdot-}$ and $^{\cdot}O_2^-$. With the progression of the reaction, a progressive increase in the content of the three free radicals ($^{\cdot}OH$, $SO_4^{\cdot-}$ and $^{\cdot}O_2^-$) was observed (as shown in Additional file 1: Fig. S7). This observation could be explained by the persistent activation of PS by the materials, resulting in an elevated generation of free radicals and significantly enhancing the degradation of phenol.

$$A_{suface}\text{-}OOH + S_2O_8^{2-} \rightarrow A_{suface} - OO^{\cdot} + SO_4^{\cdot-} + HSO_4^- \quad (7)$$

$$A_{suface}\text{-}OH + S_2O_8^{2-} \rightarrow A_{suface} - O\cdot + SO_4^{\cdot-} + HSO_4^- \quad (8)$$

$$SO_4^{\cdot-} + OH^- \rightarrow SO_4^{2-} + {}^{\cdot}OH \quad (9)$$

where A is the BC or composites; A_{suface}-$OO^{\cdot}$ and A_{suface}-$O^{\cdot}$ are radicals.

Secondly, to further elucidate the reaction mechanism, experiments designed to quench the active species were conducted to assess the roles of various types of active species in the reaction. Typically, METH was used as a quencher to scavenge $^{\cdot}OH$ and $SO_4^{\cdot-}$, and TBA was used to specifically scavenge $^{\cdot}OH$ radicals. Figure 5c demonstrates that the phenol removal rate was reduced with the addition of quenchers in the BC/PS system, indicating that the pristine biochar was not only dependent on its adsorption capacity in phenol removal, but also closely related to the production of free radicals in the system.

In the three composites with PS systems, the addition of METH and TBA significantly inhibited the phenol degradation. However, compared to METH, TBA showed stronger inhibition, this occurrence could be ascribed to the following aspects: for one, large amounts of $SO_4^{\cdot-}$ in the system were converted to $^{\cdot}OH$ radicals, and due to the extremely high rate of reaction (7.0×10^7 M^{-1} s^{-1}) (Tang et al. 2018), the actual number of $SO_4^{\cdot-}$ radicals involved in the reaction was low, which corresponded to the EPR test results. Meanwhile, in the process of quenching the radicals with METH, alcohol radicals ($CH_2OH^{\cdot}$) might be generated, which could be participated directly to degrade phenol, thus partially compensating for the degradation of phenol (Yu et al. 2019). Therefore, the quenching effect of METH was relatively weak; moreover, the strong hydrophilicity of METH hindered its efficient adsorption onto the surface of material, whereas the free radicals ($^{\cdot}OH$ and $SO_4^{\cdot-}$) produced at the surface of material would tend to adhere there and react with the pollutants, resulting in the inability of METH to give full play to its quenching effect (Zhang et al. 2020). Overall, these results demonstrated the coexistence of $SO_4^{\cdot-}$ and $^{\cdot}OH$ radicals, where the $^{\cdot}OH$ radicals were more significant, comprising 50.7% of the total contribution to the phenol degradation efficiency within the N/BM-SD/BC/PS system. To ascertain the potential involvement of $^{\cdot}O_2^-$, CF was used as a bursting agent for the experiments. Figure 5c demonstrates that as the result of inhibitory action of CF, the $^{\cdot}O_2^-$ did participate in the reaction and contributed to the phenol degradation, accounting for 25.3% of the phenol elimination within the N/BM-SD/BC/PS system. Similarly, L-His was chosen as a quencher for $^1O_2$ and the results showed that the phenol removal was not significantly reduced in the presence of L-His, further confirming the absence of $^1O_2$ in the systems.

Thirdly, recent reports have shown that Fe(IV) may be present and involved in the reaction process in iron-based AOPs (Wang et al. 2024). To verify the presence of Fe(IV), the PMSO was commonly added to quantify Fe(IV). As PMSO was converted to $PMSO_2$ via an oxygen-atom transfer step with Fe(IV), this was significantly different from the free radical-based oxidation pathway (Li et al. 2024). Additional file 1: Fig. S8 illustrates PMSO degradation and $PMSO_2$ generation in different materials/PS systems. Among them, no $PMSO_2$ generation was detected in the BC/PS system; whereas, there was a trace

amount of $PMSO_2$ generation in the BM-SD/BCs/PS system, indicating the presence of Fe(IV) in those system. Meanwhile, since PMSO and DMSO could be oxidized by Fe(IV) to generate the corresponding sulfone, thus weakening the role of Fe(IV) in the system, PMSO and DMSO could also be considered as quenchers of Fe(IV). Based on this, the effect of the presence of PMSO and DMSO on the phenol degradation performance of the system was further investigated (Fig. 5c). The results showed that the removal of phenol by the BM-SD/BCs/PS system was only slightly reduced in the presence of PMSO and DMSO, which indicated that Fe(IV) did not play an important role in the degradation of phenol despite its presence in the system.

3.3.3 Analysis of reaction intermediates

To further elucidate the degradation mechanism of phenol, the reaction intermediates in the N/BM-SD/BC/PS system were analyzed by LC–MS. As shown in Additional file 1: Fig. S9, the peak of phenol (m/z = 94) was significantly attenuated after treatment with this system, while several new peaks appeared, which corresponded to the intermediates of phenol degradation, such as P-benzoquinone, O-benzoquinone, fumaric acid, and maleic acid, respectively (Additional file 1: Table S4 for details). These results indicated that phenol was efficiently transformed in this system. Based on the results of LC–MS and EPR experiments, we proposed the degradation pathway for phenol (Additional file 1: Fig. S10): firstly, the 2nd or 4th carbon atom on the phenol molecule was attacked by ·OH or $\cdot O_2^-$ radicals to produce catechol or hydroquinone (Li et al. 2020). Subsequently, the O–H bonds in these products were further attacked to produce O-benzoquinone and P-benzoquinone. Next, the benzene ring in these intermediates was further subjected to attacks by free radicals, resulting in ring opening of the benzene ring to produce ring-opening products and small-molecule acids (e.g., fumaric, maleic, and oxalic acids) (Khoshtinat et al. 2021), which were ultimately degraded to CO_2 and H_2O.

In summary, different ball milling atmospheres significantly affected the physicochemical properties of the BM-SD/BCs composites in several ways, thereby modulating their reactivity in PS activation (Fig. 6). Firstly, ball milling under different atmospheres affected the surface structure, specific surface area and pore structure of the materials, altering the opportunities for contact with contaminants and oxidants. Secondly, the anoxic atmospheres (nitrogen and vacuum atmospheres) elevated the proportion of Fe(II) in the materials and enhanced the generation of free radicals. In addition, the nitrogen atmosphere effectively promoted the stability and distribution of functional groups, which were beneficial in facilitating electron transfer during the reaction process. Together, these properties enabled the BM-SD/BCs prepared with different atmospheres to exhibit different catalytic activities, contributing to the understanding and optimization of the potential application of this composite in advanced oxidation processes.

3.4 Potential practicability of BM-SD/BCs

In order to investigate the potential application of BM-SD/BCs, the concentrations of Fe(II) and Fe(III) in the reaction system were first quantitatively analyzed by phenanthroline spectrophotometry. As expected, no iron leaching was detected in the BC/PS system due to the

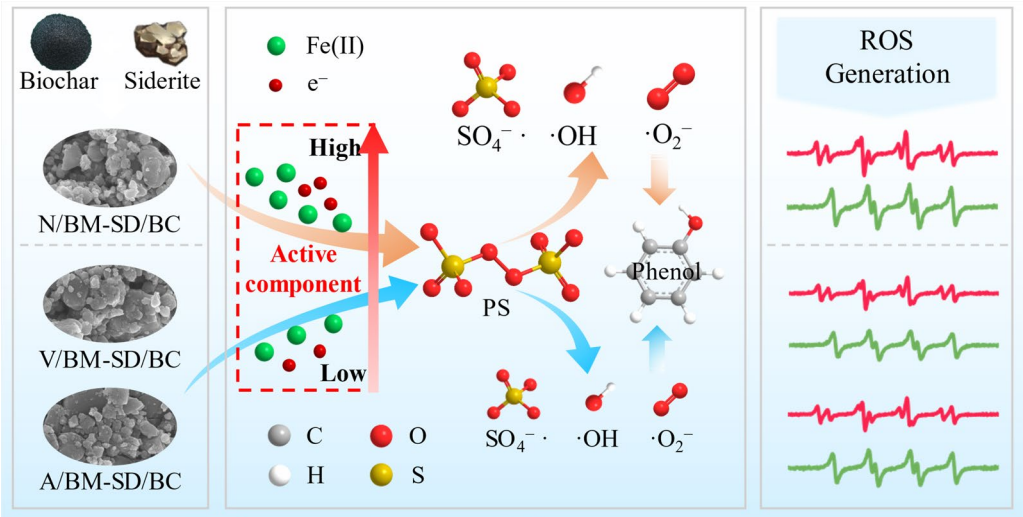

Fig. 6 Effects of different ball milling atmospheres on the properties and activities of BM-SD/BCs

extremely minute amount of iron content, as shown in Additional file 1: Fig. S11a. In contrast, slight iron leaching was observed in the BM-SD/BCs/PS systems with total iron concentrations of 1.08 mg L^{-1} (A/BM-SD/BC/PS), 1.28 mg L^{-1} (N/BM-SD/BC/PS), and 1.22 mg L^{-1} (V/BM-SD/BC/PS). It was noteworthy that Fe(III) accounted for more than 85% of the total Fe leached in these three BM-SD/BCs/PS systems. This phenomenon was likely due to the participation of leached Fe(II) in the PS activation process, which in turn was oxidized to Fe(III). More critically, these leached Fe ion concentration levels were below the EU's discharge standards for Fe (2 mg L^{-1}) (Zhao et al. 2022). This result strongly confirmed the environmental compatibility of BM-SD/BCs .

To further evaluate the durability of N/BM-SD/BC, the continuous flow reactor consisting of catalyst-filled columns was constructed. As shown in Additional file 1: Fig. S11b, the removal rate of phenol was maintained at 100% for the first 5 h of continuous operation, which demonstrated an extremely efficient pollutant degradation capability. However, with the increase of operation time, the removal rate began to decrease gradually. The removal rate was stabilized at 70% in the 36th h, and then decreased to 45% in the 72nd h. This might be attributed to the fact that some intermediates generated during the reaction process adsorbed and occupied the active sites of the catalysts, thus inhibiting the catalytic activity. Even so, from the overall experimental results, N/BM-SD/BC still showed excellent pollutant degradation durability under PS activation conditions. This means that N/BM-SD/BC is expected to maintain stable catalytic performance for a long period of time and degrade pollutants efficiently under PS activation conditions in practical application scenarios.

4 Conclusions

In this study, we systematically investigated the modulation effect of ball milling atmosphere on the physicochemical properties and catalytic activity of the siderite/biochar composites (BM-SD/BCs). It was shown that N/BM-SD/BC prepared under nitrogen atmosphere exhibited the best catalytic performance in PS-activated degradation of phenol, which was significantly better than that of the composites under air and vacuum environments. This enhancement mainly stems from the fact that the nitrogen environment effectively reduces the oxidation of Fe(II), enhances the reducing activity of the materials, and promotes the exposure of surface functional groups, providing ideal conditions for radical generation and electron transfer. Taken together, the remarkable modulation of material activity and structural properties by ball milling atmosphere reveals that ball milling atmosphere can be used as an important design variable in the synthesis and optimization of highly efficient environmental catalysts, which provides a new direction for the research and application of persulfate activation and pollutant degradation.

Supplementary Information

The online version contains supplementary material available at https://doi.org/10.1007/s42773-025-00474-y.

Additional file 1.

Author contributions

Hui Zhang: Methodology, visualization, formal analysis, investigation, data curation, writing—original draft; Zi Cheng: Visualization, methodology, formal analysis; Kai Hu: Investigation, methodology; Boxiong Shen: Formal analysis, methodology; Honghong Lyu: Conceptualization, formal analysis, funding, writing—review and editing; Jingchun Tang: Funding, writing—review and editing. All authors read and approved the final manuscript.

Funding

This work was supported by the (1) Science Fund for Distinguished Young Scholars of Tianjin [23JCJQJC00120]; (2) National Natural Science Foundation of China [42377225, 42477524]; and (3) 111 program, Ministry of Education, China [T2017002].

Data availability

The datasets used and analyzed during the current study available from the corresponding author on reasonable request.

Declarations

Competing interests

The authors have no competing interests to declare that are relevant to the content of this article.

Author details

[1]Tianjin Key Laboratory of Clean Energy and Pollution Control, School of Energy and Environmental Engineering, Hebei University of Technology, Tianjin 300401, China. [2]MOE Key Laboratory of Pollution Processes and Environmental Criteria/Tianjin Engineering Research Center of Environmental Diagnosis and Contamination Remediation, College of Environmental Science and Engineering, Nankai University, Tianjin 300350, China.

Received: 19 November 2024 Revised: 28 April 2025 Accepted: 11 May 2025
Published online: 17 June 2025

References

Acisli O, Khataee A, Darvishi Cheshmeh Soltani R, Karaca S (2017) Ultrasound-assisted Fenton process using siderite nanoparticles prepared via planetary ball milling for removal of reactive yellow 81 in aqueous phase. Ultrason Sonochem 35:210–218

Chen X, Zhu J, Ma Y, Zeng C, Mu R, Deng Z, Zhang Z (2024a) Facile synthesis of ball-milling and oxalic acid co-modified sludge biochar to efficiently activate peroxymonosulfate for sulfamethoxazole degradation: $^1O_2$ and surface-bound radicals. J Hazard Mater 465:133026

Chen H, Gao J, Wang Q, Liu Y, Fu X, Guo Y, Wang H, Wang Y, An J (2024b) Natural pyrite and ascorbic acid co-enhance periodate activation for inactivation of antibiotic resistant bacteria and inhibition of resistance genes transmission: a green disinfection process dominated by singlet oxygen. J Hazard Mater 477:135217

Cheng Z, Lyu H, Shen B, Tian J, Sun Y, Wu C (2022) Removal of antimonite (Sb(III)) from aqueous solution using a magnetic iron-modified carbon

nanotubes (CNTs) composite: experimental observations and governing mechanisms. Chemosphere 288:132581
Cheng Z, Lyu H, Huang Y, Shen B, Tang J (2024) Metal cations enhanced the bonding of Sb(V) on adsorbent surfaces: An effective strategy for adsorbent engineering. Chem Eng J 479:147630
Dai X-H, Fan H-X, Yi C-Y, Dong B, Yuan S-J (2019) Solvent-free synthesis of a 2D biochar stabilized nanoscale zerovalent iron composite for the oxidative degradation of organic pollutants. J Mater Chem A 7:6849–6858
Damiri F, Dobaradaran S, Hashemi S, Foroutan R, Vosoughi M, Sahebi S, Ramavandi B, Camilla Boffito D (2020) Waste sludge from shipping docks as a catalyst to remove amoxicillin in water with hydrogen peroxide and ultrasound. Ultrason Sonochem 68:105187
Dong C-D, Chen C-W, Hung C-M (2017) Synthesis of magnetic biochar from bamboo biomass to activate persulfate for the removal of polycyclic aromatic hydrocarbons in marine sediments. Biores Technol 245:188–195
Duan X, Sun H, Kang J, Wang Y, Indrawirawan S, Wang S (2015) Insights into heterogeneous catalysis of persulfate activation on dimensional-structured nanocarbons. ACS Catal 5:4629–4636
Gao P, Fan X, Sun D, Zeng G, Wang Q, Wang Q (2024) Recent advances in ball-milled materials and their applications for adsorptive removal of aqueous pollutants. Water 16:1639
Giannakis S, Lin K-YA, Ghanbari F (2021) A review of the recent advances on the treatment of industrial wastewaters by sulfate radical-based advanced oxidation processes (SR-AOPs). Chem Eng J 406:127083
He J, Xiao Y, Tang J, Chen H, Sun H (2019) Persulfate activation with sawdust biochar in aqueous solution by enhanced electron donor-transfer effect. Sci Total Environ 690:768–777
Huang J, Jones A, Waite TD, Chen Y, Huang X, Rosso KM, Kappler A, Mansor M, Tratnyek PG, Zhang H (2021) Fe(II) redox chemistry in the environment. Chem Rev 121:8161–8233
Khoshtinat F, Tabatabaie T, Ramavandi B, Hashemi S (2021) Phenol removal kinetics from synthetic wastewater by activation of persulfate using a catalyst generated from shipping ports sludge. Chemosphere 283:131265
Kumar M, Xiong X, Wan Z, Sun Y, Tsang DCW, Gupta J, Gao B, Cao X, Tang J, Ok YS (2020) Ball milling as a mechanochemical technology for fabrication of novel biochar nanomaterials. Bioresour Technol 312:123613
Lee J, von Gunten U, Kim J-H (2020) Persulfate-based advanced oxidation: critical assessment of opportunities and roadblocks. Environ Sci Technol 54:3064–3081
Li L, Wu H, Chen H, Zhang J, Xu X, Wang S, Wang S, Sun H (2020) Heterogeneous activation of peroxymonosulfate by hierarchically porous cobalt/iron bimetallic oxide nanosheets for degradation of phenol solutions. Chemosphere 256:127160
Li G, Zhang Y, Zhang X, Zhang J, Sun B (2024) Deciphering the formation of Fe(IV) in the Fe(II)/peroxydisulfate process: the critical role of sulfate radical. Environ Sci Technol 58:15864–15873
Liu L, Xu X, Li Y, Su R, Li Q, Zhou W, Gao B, Yue Q (2020) One-step synthesis of "nuclear-shell" structure iron-carbon nanocomposite as a persulfate activator for bisphenol A degradation. Chem Eng J 382:122780
Liu W, Liu N, Song K, Zeng M, Lu Z (2024) Fabrication of WO_3 photocatalyst by plasma assisted ball milling under different discharge atmospheres. Vacuum 220:112809
Lyu H, Gao B, He F, Ding C, Tang J, Crittenden JC (2017a) Ball-milled carbon nanomaterials for energy and environmental applications. ACS Sustain Chem Eng 5:9568–9585
Lyu H, Tang J, Huang Y, Gai L, Zeng EY, Liber K, Gong Y (2017b) Removal of hexavalent chromium from aqueous solutions by a novel biochar supported nanoscale iron sulfide composite. Chem Eng J 322:516–524
Lyu H, Gao B, He F, Zimmerman AR, Ding C, Tang J, Crittenden JC (2018a) Experimental and modeling investigations of ball-milled biochar for the removal of aqueous methylene blue. Chem Eng J 335:110–119
Lyu H, Gao B, He F, Zimmerman AR, Ding C, Huang H, Tang J (2018b) Effects of ball milling on the physicochemical and sorptive properties of biochar: experimental observations and governing mechanisms. Environ Pollut 233:54–63
Ma Y, Yao Y, Deng Z, Tang J, Liu Y, Ma J, Zhang Z (2024) Ball milling and phosphoric acid hydrothermally co-functionalized sludge biochar for efficiently adsorptive removal of environmental concentration sulfamethoxazole: experimental, characterization and DFT study. Sep Purif Technol 328:125051
Meng Y, Chen X, Ai D, Wei T, Fan Z, Wang B (2022) Sulfur-doped zero-valent iron supported on biochar for tetracycline adsorption and removal. J Clean Prod 379:134769
Naghdi M, Taheran M, Brar SK, Rouissi T, Verma M, Surampalli RY, Valero JR (2017) A green method for production of nanobiochar by ball milling-optimization and characterization. J Clean Prod 164:1394–1405
Nasrullah A, Khan AS, Bhat AH, Din IU, Inayat A, Muhammad N, Bakhsh EM, Khan SB (2021) Effect of short time ball milling on physicochemical and adsorption performance of activated carbon prepared from mangosteen peel waste. Renew Energy 168:723–733
Rong X, Xie M, Kong L, Natarajan V, Ma L, Zhan J (2019) The magnetic biochar derived from banana peels as a persulfate activator for organic contaminants degradation. Chem Eng J 372:294–303
Sun Y, Sun P, Niu S, Shen B, Lyu H (2024) Atmosphere matters: The protection of wet ball milling instead of dry ball milling accelerates the electron transfer effect of sulfurized micron iron/biochar to Cr(VI). Chem Eng J 490:151738
Tang L, Liu Y, Wang J, Zeng G, Deng Y, Dong H, Feng H, Wang J, Peng B (2018) Enhanced activation process of persulfate by mesoporous carbon for degradation of aqueous organic pollutants: electron transfer mechanism. Appl Catal B 231:1–10
Tang J, Zhao B, Lyu H, Li D (2021) Development of a novel pyrite/biochar composite (BM-FeS_2@BC) by ball milling for aqueous Cr(VI) removal and its mechanisms. J Hazard Mater 413:125415
Thi-Hai Anh N, Oh S-Y (2019) Biochar-mediated oxidation of phenol by persulfate activated with zero-valent iron. J Chem Technol Biotechnol 94:3932–3940
Wang H, Guo W, Yin R, Du J, Wu Q, Luo H, Liu B, Sseguya F, Ren N (2019) Biochar-induced Fe(III) reduction for persulfate activation in sulfamethoxazole degradation: insight into the electron transfer, radical oxidation and degradation pathways. Chem Eng J 362:561–569
Wang P, Hu J, Liu T, Han G, Ma W-M, Li J (2023) New insights into ball-milled zero-valent iron composites for pollution remediation: an overview. J Clean Prod 385:135513
Wang Q, Sun Y, Hao M, Yu F, Houda C (2024) Persistent degradation of 2,4-dichlorophenol in groundwater by persulfate synergize with Fe(III)/$CaSO_3$ system: role of Fe(IV) and $^1O_2$ oxidation. Sep Purif Technol 334:125979
Xiao Y, Lyu H, Tang J, Wang K, Sun H (2020a) Effects of ball milling on the photochemistry of biochar: enrofloxacin degradation and possible mechanisms. Chem Eng J 384:123311
Xiao S, Cheng M, Zhong H, Liu Z, Liu Y, Yang X, Liang Q (2020b) Iron-mediated activation of persulfate and peroxymonosulfate in both homogeneous and heterogeneous ways: a review. Chem Eng J 384:123265
Xu X, Xu Z, Huang J, Gao B, Zhao L, Qiu H, Cao X (2021) Sorption of reactive red by biochars ball milled in different atmospheres: co-effect of surface morphology and functional groups. Chem Eng J 413:127468
Yang X, Wan Y, Zheng Y, He F, Yu Z, Huang J, Wang H, Ok YS, Jiang Y, Gao B (2019) Surface functional groups of carbon-based adsorbents and their roles in the removal of heavy metals from aqueous solutions: a critical review. Chem Eng J 366:608–621
Yang X, Liu S, Liang T, Yan X, Zhang Y, Zhou Y, Sarkar B, Ok YS (2022) Ball-milled magnetite for efficient arsenic decontamination: Insights into oxidation–adsorption mechanism. J Hazard Mater 427:128117
Yin R, Guo W, Wang H, Du J, Wu Q, Chang J-S, Ren N (2019) Singlet oxygen-dominated peroxydisulfate activation by sludge-derived biochar for sulfamethoxazole degradation through a nonradical oxidation pathway: performance and mechanism. Chem Eng J 357:589–599
Yu J, Tang L, Pang Y, Zeng G, Wang J, Deng Y, Liu Y, Feng H, Chen S, Ren X (2019) Magnetic nitrogen-doped sludge-derived biochar catalysts for persulfate activation: internal electron transfer mechanism. Chem Eng J 364:146–159
Zhang H, Chen S, Zhang H, Fan X, Gao C, Yu H, Quan X (2019) Carbon nanotubes-incorporated MIL-88B-Fe as highly efficient Fenton-like catalyst for degradation of organic pollutants. Front Environ Sci Eng 13:1–11
Zhang H, Tang L, Wang J, Yu J, Feng H, Lu Y, Chen Y, Liu Y, Wang J, Xie Q (2020) Enhanced surface activation process of persulfate by modified bagasse biochar for degradation of phenol in water and soil: active sites and electron transfer mechanism. Colloids Surf A 599:124904

Zhao L, Zhang H, Zhao B, Lyu H (2022) Activation of peroxydisulfate by ball-milled α-FeOOH/biochar composite for phenol removal: component contribution and internal mechanisms. Environ Pollut 293:118596
Zhen Y, Zhu S, Sun Z, Tian Y, Li Z, Yang C, Ma J (2021) Identifying the persistent free radicals (PFRs) formed as crucial metastable intermediates during peroxymonosulfate (PMS) activation by N-doped carbonaceous materials. Environ Sci Technol 55:9293–9304
Zhong C, Jiang Y, Liu Q, Sun X, Yu J (2023) Natural siderite derivatives activated peroxydisulfate toward oxidation of organic contaminant: a green soil remediation strategy. J Environ Sci 127:615–627